materials

MDPI

Article

Improving the Photocatalytic Activity of Ti_3C_2 MXene by Surface Modification of N Doped

Lidan Cui [1], Jianfeng Wen [1,*], Quanhao Deng [1], Xin Du [1], Tao Tang [1], Ming Li [1], Jianrong Xiao [1], Li Jiang [1], Guanghui Hu [1], Xueli Cao [1] and Yi Yao [2,*]

[1] Key Laboratory of Low-Imensional Structural Physics and Application, Education Department of Guangxi Zhuang Autonomous Region, College of Science, Guilin University of Technology, Guilin 541004, China; cld930429@163.com (L.C.)

[2] Guangxi Collaborative Innovation Center for Water Pollution Control and Water Safety in Karst Areas, College of Environmental Science and Engineering, Guilin University of Technology, 319 Yanshan Street, Guilin 541004, China

* Correspondence: 2005026@glut.edu.cn (J.W.); yaoyi117@163.com (Y.Y.)

Abstract: Methyl orange dye (MO) is one of the azo dyes, which is not only difficult to degrade but also hazardous to human health, therefore, it is necessary to develop an efficient photocatalyst to degrade MO. In this paper, a facile and low-cost elemental doping method was used for the surface modification of Ti_3C_2 MXene, i.e., nitrogen-doped titanium carbide was used as the nitrogen source, and the strategy of combining solvent heat treatment with non-in situ nitrogen doping was used to prepare N-Ti_3C_2 MXene two-dimensional nanomaterials with high catalytic activity. It was found that the catalytic efficiency of N-Ti_3C_2 MXene materials was enhanced and improved compared to the non-doped Ti_3C_2 MXene. In particular, N-Ti_3C_2 1:8 MXene showed the best photo-catalytic ability, as demonstrated by the fact that the N-Ti_3C_2 1:8 MXene material successfully degraded 98.73% of MO (20 mg/L) under UV lamp irradiation for 20 min, and its catalytic efficiency was about ten times that of Ti_3C_2 MXene, and the N-Ti_3C_2 photo-catalyst still showed good stability after four cycles. This work shows a simplified method for solvent heat-treating non-in situ nitrogen-doped Ti_3C_2 MXene, and also elaborates on the photo-catalytic mechanism of N-Ti_3C_2 MXene, showing that the high photo-catalytic effect of N-Ti_3C_2 MXene is due to the synergistic effect of its efficient charge transfer and surface-rich moieties. Therefore, N-Ti_3C_2 MXene has a good prospect as a photo-catalyst in the photocatalytic degradation of organic pollutants.

Keywords: photo-catalytic; solvent heat treatment; N-Ti_3C_2 MXene; Methyl Orange Removal

Citation: Cui, L.; Wen, J.; Deng, Q.; Du, X.; Tang, T.; Li, M.; Xiao, J.; Jiang, L.; Hu, G.; Cao, X.; et al. Improving the Photocatalytic Activity of Ti_3C_2 MXene by Surface Modification of N Doped. *Materials* **2023**, *16*, 2836. https://doi.org/10.3390/ma16072836

Academic Editors: Stanisław Wacławek and Daniele Silvestri

Received: 23 February 2023
Revised: 21 March 2023
Accepted: 22 March 2023
Published: 2 April 2023

1. Introduction

With the progressive increase in population and the rapid expansion of business over the past decade, various types of domestic sewage and industrial wastewater have rapidly increased, making the water pollution problem more serious and causing serious damage to the ecological environment [1–3]. In particular, azo dyes are discharged from wastewater due to their anti-biodegradability. Excessive amounts of azo dyes are teratogenic, mutagenic, and carcinogenic, posing a highly toxic hazard to plants, animals, and humans [4,5] Therefore, there is an urgent need for efficient and cost-effective water treatment technologies. So far, many methods have been developed, such as adsorption, redox photochemical degradation, membrane filtration, and photocatalysis [6,7] have been widely used to remove pollutants from water. Among them, photocatalytic technology is gaining popularity owing to its several benefits, which include environmental friendliness, high efficiency, stability, and a high degradation rate [8,9].

MXenes [10], a novel two-dimensional substance, has several applications in photocatalysis [11] and high electrical conductivity owing to its enormous specific surface area [12], many active sites [13], and the presence of numerous functional groups (-O,

-OH, -F, etc.) with good hydrophobicity and controllable interlayer distances [14–17]. MXenes follow the general formula of $M_{n+1}X_nT_x$, where n+1 (n = 1, 2, 3) is the early transition metal layer, and M is intercalated with n layers of carbon or nitrogen X. Since the first report of MXene in 2011 [18], more than 30 MXene such as Ti_3C_2, Ti_3CN, TiNbC, V_2C, Mo_2C, Nb_2C, and Y_2CF_2 have been successfully prepared [19–21]. The general MXene is obtained by the selective removal of atoms from the MAX phase by treatment with hydrofluoric acid or other fluorine sources. The precursors of MXene MAX phase are a collective term for a ternary layered ceramic material, where M is a pre-transition metal (e.g., Ti, Sr, V, Nb, Cr, Ta, Zr, Mo, etc.), A is the main group II or IV element, and X is C or N, etc. [22–27]. Ti_3C_2, a member of the MXenes family, has superior electrical conductivity, a large specific surface area, and many active sites, which may result in the separation and transmission of photoexcited electron-hole pairs. At the same time, it is simple to create composite materials using Ti_3C_2 and other photo-catalysts because of their excellent flexibility and distinctive layered structure. In the case of Ti_3C_2 composites, Ti_3C_2 not only increases the absorption of light by its blackbody but also causes rapid carrier migration and inhibits its compounding [28]. Therefore, Ti_3C_2 is often utilized as an alternative noble metal [29] co-catalyst to boost the complexes' photo-catalytic activity [30–33]. We note that it has been reported in the literature that Ti_3C_2 with -F and -OH end groups are a narrow band gap semiconductor [34], and considering that Ti_3C_2 exfoliated from HF acid liquid phase will have -F and -OH end groups and may also have photo-catalytic properties. Therefore, we investigated the photocatalytic activity of Ti_3C_2. Unfortunately, the photosynthesis performance of Ti_3C_2 itself was not satisfactory.

Considering that Ti_3C_2 can be improved by changing the elemental composition and adjusting the surface functional groups to improve the performance of two-dimensional accordion-like Ti_3C_2 nanomaterials, we used the surface modification of Ti_3C_2 utilizing introducing heteroatoms to investigate its photocatalytic properties. It has been discovered that ecologically friendly urea (CH_4N_2O) in high-concentration nitrogen alcohol is an effective source of liquid nitrogen doping and that the liquid N doping source can retain excellent contact with Ti_3C_2 to achieve high N doping without stacking N-Ti_3C_2 nanospheres [35,36]. The modulation of nitrogen-doped Ti_3C_2 nanomaterials is greatly enhanced in terms of carrier density, surface energy, and surface reactivity.

Currently, there are many research reports on N-Ti_3C_2 in the fields of batteries [37], capacitors [38], and electrocatalysis [39], however, there are fewer reports on the application of N-Ti_3C_2 in the field of photocatalysis. Thus, in this paper, urea-saturated alcohol solution as a liquid nitrogen source, and a simple and controllable strategy combining solvent thermal treatment and non-in situ nitrogen doping were used to prepare N-Ti_3C_2 MXene 2D nanomaterials with high catalytic activity. Transforming the usual way of N-Ti_3C_2 nanomaterials, we applied it as the main catalyst for the first time in the field of photocatalysis and confirmed that it could significantly improve the photocatalytic degradation of MO. In addition, the morphological and physicochemical properties of the materials were thoroughly examined, and the reaction mechanism of the photo-catalysts was discussed through experimental and theoretical studies.

2. Materials and Methods

2.1. Preparation of N-Ti_3C_2 Catalyst

Ti_3AlC_2 (99.7%), urea (AR), dimethyl sulfoxide (DMSO, AR), hydrofluoric acid (HF, AR), and anhydrous ethanol (99.5%) were purchased from Guilin Bell Experimental Equipment Co. All chemical reagents were analytical grade without additional purification, and all experiments utilized clean water.

The synthetic roadmap of the N-Ti_3C_2 catalyst is shown in Figure 1, and its structure is schematically shown in Figure 2.

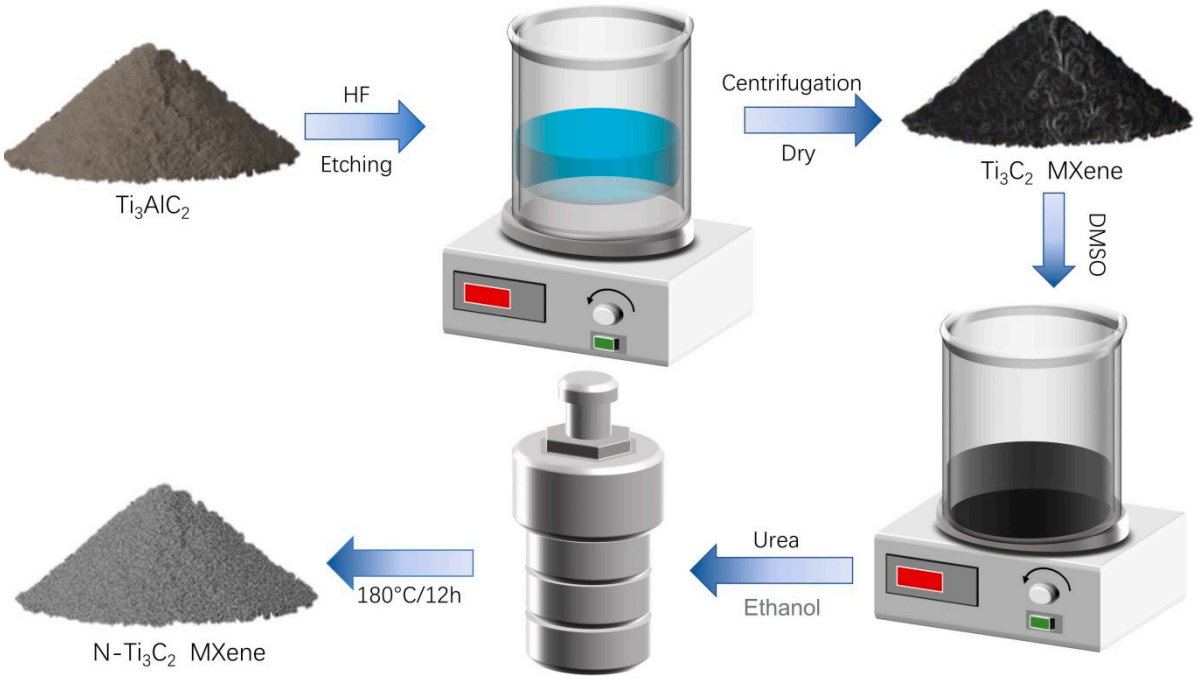

Figure 1. Roadmap for the synthesis of N−Ti_3C_2 catalyst.

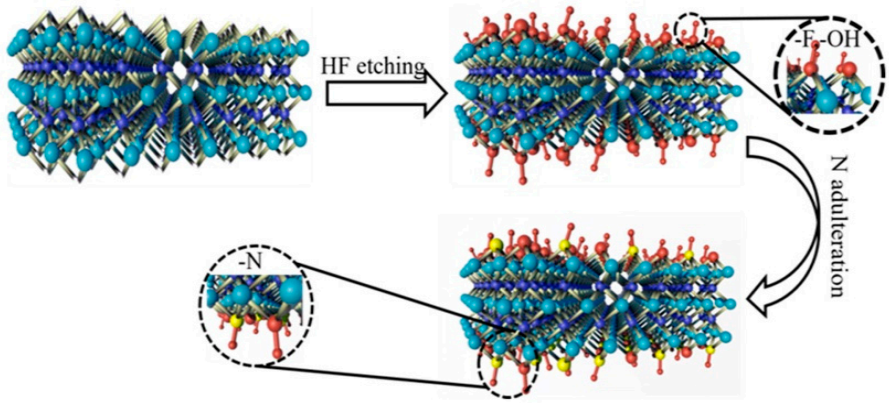

Figure 2. Schematic diagram of the synthetic structure of N−Ti_3C_2 catalyst.

Synthesis of Ti_3C_2: Ti_3C_2 was synthesized by etching off the aluminum element in Ti_3AlC_2. Firstly, 2 g Ti_3AlC_2 powder was mixed with 20 mL of 30% hydrofluoric acid at room temperature for 5 h. Secondly, the etched material was centrifuged by centrifuge to collect the black powder and washed with deionized water to a pH of about 6–7, and placed in a dryer for 12 h at 60 °C.

The synthesis route of N-doped Ti_3C_2: Firstly, 0.5 g of the above-dried Ti_3C_2 was placed in 15 mL of dimethyl sulfoxide (DMSO) and agitated for 24 h for intercalation. The powder was recovered by centrifugation, washed several times with deionized water, and then dried for 12 h at 60 °C in a drier. Next, take the intercalated Ti_3C_2 and urea in the ratio of 8:1 put it into 60 mL anhydrous ethanol for mixing, put it into the ultrasonic machine for 30 min to mix well, and transfer it to the stainless-steel autoclave lined with polytetrafluoroethylene for solvent heat reaction at 180 °C for 12 h. Finally, the material in the reaction kettle was collected by centrifugation, washed with deionized water and anhydrous ethanol until the pH was about neutral, and put into a dryer for 12 h at 60 °C to obtain N-doped Ti_3C_2 powder.

2.2. Materials Characterization

By using energy-dispersive X-ray spectroscopy (EDS) detectors and a field emission scanning electron microscope (FESEM, SU5000, Hitachi, Tokyo, Japan), researchers were able to examine the morphological characteristics and elemental composition of the samples. X-ray photoelectron spectroscopy (XPS, ESCALAB-250XI) analyzed the valence and chemical composition of the elements. X-ray diffraction spectroscopy (XRD, Bruker D8 Advanced) measured the crystal structure of the samples. Fourier infrared spectroscopy (FTIR) was used to measure the functional groups and chemical bonds on the surface of the samples. Optical properties were tested by UV-Vis spectrophotometer (DRS, Shimadzu Lambda 750, Tokyo, Japan).

2.3. Electrochemical Measurements

The prepared sample coated on FTO glass served as the working electrode, platinum wire served as the counter electrode, the $Hg/Hg_2Cl_2/KCl$ (saturated) electrode served as a reference, and 0.5 mol/L aqueous solution served as the electrolyte, photochemical measurements were carried out using an electrochemical workstation (CHI860B). The produced photocurrent was measured while a solar simulator was irradiated with a 10-s lamp on/off cycle. The irradiation intensity was 1000 W/m^2 and the effective area of the sample was 1 cm^2.

2.4. Photocatalytic Performance

The photocatalytic performance of N-Ti_3C_2 was tested by methyl orange dye MO degradation. The sample numbers obtained at different scales will be used in this experiment, and the light source used is a 1000 W mercury lamp (Wavelength range 320 nm–390 nm, main peak value 365 nm) to emit ultraviolet light. Take 50mL of methyl orange dye with a concentration of 20 mg/L mixed with 50 mg N-Ti_3C_2 and pour it into the test tube, sonicate for some time to make it mix evenly, and then put it into a photochemical reactor (BL-GHX-1D) and stir under dark conditions for 30 min to achieve adsorption resolution equilibrium, turn on the light source and take 3–4 mL every 10 min. The resulting solutions were detected with a UV-Vis spectrophotometer for absorbance at 464 nm (characteristic wavelength of MO) to determine the degree of degradation.

3. Results and Discussion

3.1. SEM and EDS Analysis

In the chemical etching of aluminum in Ti_3AlC_2 as shown in Figure 3a,b, SEM can observe that Ti_3C_2 MXene shows a unique accordion-like multilayer structure, revealing the effective production of Ti_3C_2 through HF etching of Ti_3AlC_2. It is well known that at a certain temperature and high pressure, due to the low boiling point and high mobility of ethanol, it may easily lead to the diffusion of urea molecules into the interlayer space during the solvent heat treatment. The morphology of the nitrogen-doped Ti_3C_2 MXene is shown in Figure 3c,d was also well preserved after the solvent thermal reaction, in which the spacing between some of the layers became larger, the surface of the sample was rougher and more complex, and the layer surface was attached with uniform and fine nanoparticles. To further elucidate the structure of N-Ti_3C_2 MXene nanomaterial, EDS elemental mapping of individual elements in N-Ti_3C_2 MXene nanomaterial was performed (Figure 3e), and X-ray spectra (EDS) showed that Ti, C, N, F, and O elements were uniformly distributed in the prepared samples. These characterizations strongly demonstrate the successful preparation of N-Ti_3C_2 MXene 2D nanomaterial. The formation of N-Ti_3C_2 expands the interlayer distance, resulting in an increased specific surface area and more active sites, which is more favorable for carrier transport and separation.

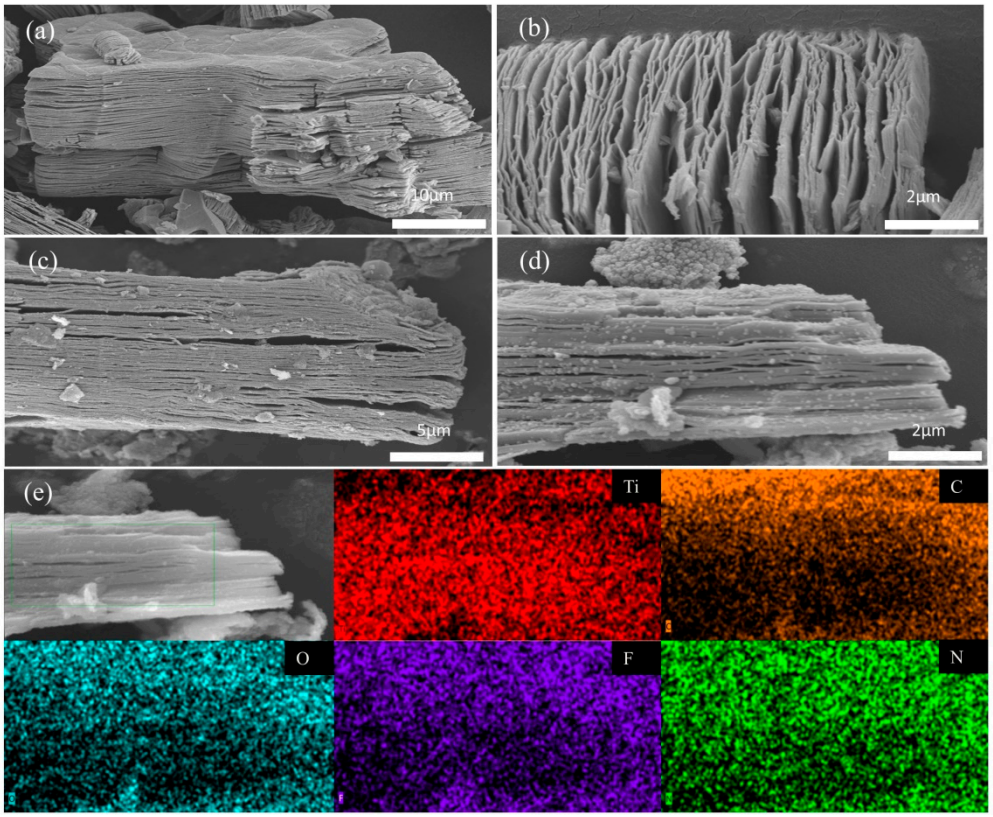

Figure 3. (**a**,**b**) Local magnifications of layered Ti_3C_2 MXene and Ti_3C_2; (**c**,**d**) SEM images of N−Ti_3C_2 MXene nanomaterials at different magnifications; (**e**) EDS elemental mapping of Ti, C, O, F and N nanomaterials of N−Ti_3C_2 MXene.

3.2. XRD and FTIR Analysis

The X-ray powder diffraction was used to examine the crystalline and phase structure of the material (XRD). As shown in Figure 4a, the typical four prominent peaks of Ti_3AlC_2 (JCPDS No. 52-0875) are distributed at 9.517°, 19.154°, 39.037°, and 60.257°, corresponding to the four crystallographic planes (002), (004), (104), and (110), respectively. The strongest XRD diffraction peak of Ti_3AlC_2 after HF etching (104) crystalline plane disappears and (002) and (004) crystalline planes are shifted to lower angles compared to Ti_3C_2. The results show that the layered Ti_3C_2 MXene was successfully prepared. with the addition of the nitrogen dopant, the diffraction peaks of the (002) crystalline plane corresponding to N-Ti_3C_2 1:2, N-Ti_3C_2 1:5, N-Ti_3C_2 1:8 and N-Ti_3C_2 1:10 shifted from 9.517° to 6.94°, 6.8°, 6.79° and 6.75° relative to Ti_3C_2 is particularly obvious. This indicates that the interlayer distance of N-Ti_3C_2 MXene increases with the doping of nitrogen, which gives it a larger specific surface area and exposes more active sites. In addition, we found diffraction peaks (101) and (211) of titanium dioxide based on XRD diffraction patterns, indicating that a small portion of titanium dioxide was also formed during the nitrogen doping process [40]. The surface functional groups and bonds of the sample were measured by Fourier infrared spectroscopy (FTIR), as shown in Figure 4b, and some surface -F groups of Ti_3C_2 were substituted by hydroxyl groups through anhydrous ethanol due to the abundance of hydroxyl groups in anhydrous ethanol, i.e., the sharp characteristic peaks near 3606 and 3738 cm^{-1} represent free -OH. Since the N atom forms polar covalent bonds with the H atom and is easily adsorbed to the Ti_3C_2 surface, the characteristic peaks near 3130 and 3109 cm^{-1} are the N-H vibrational peaks of the bonding, the vibrational peaks at 1350–1550 cm^{-1} can be attributed to the vibrational stretching of -CH_3 and the C-N stretching vibrational peaks in the urea molecule, and the characteristic peaks near 580 cm^{-1} corresponds to the stretching vibration of Ti-C. The presence of these functional groups can promote electron transfer

and enhance electrical conductivity, while the doping of N atoms can effectively improve the electron transport network and ion transport channels of Ti_3C_2 MXene materials [41].

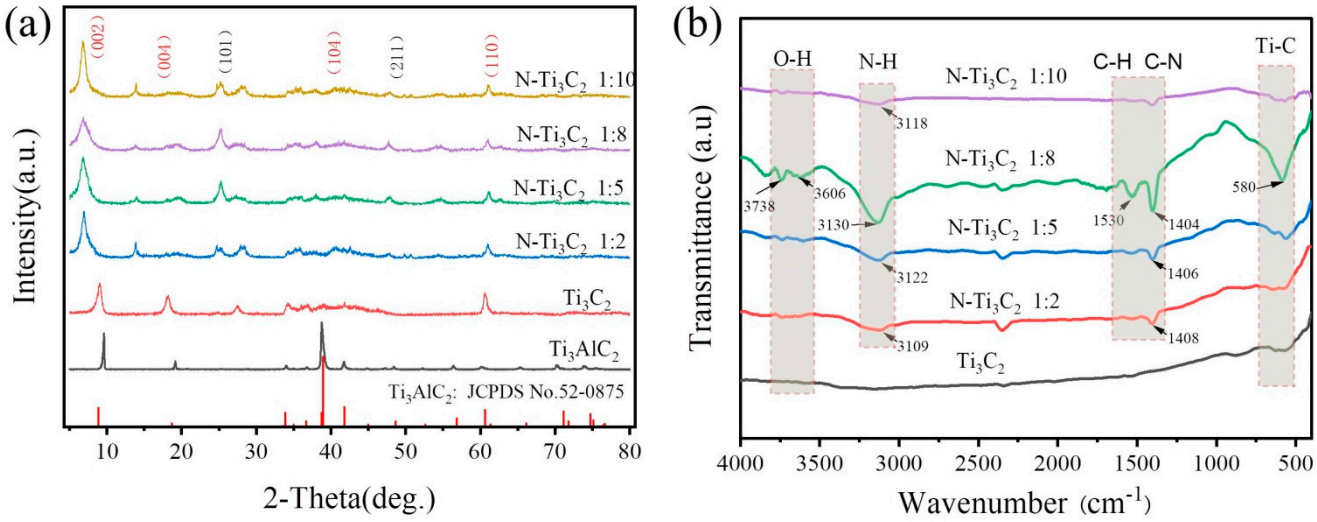

Figure 4. (**a**) XRD patterns of Ti_3C_2 MXene and N−Ti_3C_2 MXene nanomaterials; (**b**) FTIR spectra of Ti_3C_2 and N−Ti_3C_2 MXene.

3.3. XPS Analysis

X-ray photoelectron spectroscopy was used to investigate the chemical makeup and surface state of N-Ti_3C_2 MXene (XPS). As illustrated in Figure 5a. The obvious peaks of Ti, O, C, and F elements could be seen by the full scan spectrum, compared to the XPS curve of N- Ti_3C_2 material with an extra minor peak of N element. In addition, N-Ti_3C_2 materials have higher peak O element intensities than Ti_3C_2 materials, and the atomic concentration of O increases from 18.33% to 29.15%, indicating that part of Ti_3C_2 is converted to TiO_2 in the hydrothermal process. Among them, it should be noted that the atomic concentration of F is 11.9%, indicating the presence of a considerable amount of F termination groups on the surface of N-Ti_3C_2 MXene. Figure 5b represents the original Ti_3C_2 MXene with peak I at 685.0 eV representing the C-Ti-F functional group and peak II at 686.5 eV representing AlFx [42], with a shift in the peak position after nitrogen doping, probably due to a change in the elemental valence state and the appearance of a new diffraction peak, i.e., peak III at 689.18 eV, representing F-C [43]. Similarly, peak I at 529.9 eV in the O 1s region of the spectrum in Figure 5c represents the C-Ti-O functional group, peak II at 531.1 eV represents the C-O functional group, and peak III at 533.0 eV represents the C-Ti-OH functional group [44]. As shown in Figure 5d, peaks I at 455.1 eV and 461.1 eV in the Ti 2p region of the XPS spectrum of Ti_3C_2 MXene refer to the C-Ti functional group, whereas the second expanded peak II at 456.6 eV alludes to the C-Ti-F functional group [42]. In addition, the XPS spectrum of Ti 2p in N-Ti_3C_2 MXene has a new pair of peaks III (Ti 3p/2 and Ti p/2) appearing at 459.2 eV and 464.88 eV, respectively, inferred to be possibly from the oxidation product TiO_2 formed during the hydrothermal treatment [45], which corresponds to the (101) and (211) diffraction peaks found in the XRD diffraction energy spectrum corresponding to the formation of TiO_2, both confirming the formation of TiO_2. From Figure 5e, it can be seen that the XPS spectra of C 1s found in the pristine Ti_3C_2 MXene have three diffraction peaks with different valence states, which may originate from external functional groups; peak I is 282.0 eV, representing the C-Ti-(O/OH/F) functional group; peak II is 284.8 eV, representing the C-C functional group; and peak III is 286.5 eV, representing the C-Hx/C-O functional group. One more diffraction peak can be seen in the XPS spectrum of C 1s in N-Ti_3C_2 compared to Ti_3C_2 after doping with nitrogen, i.e., peak IV is 289.1 eV, representing the C-N functional group (visible in the Annex) [45].

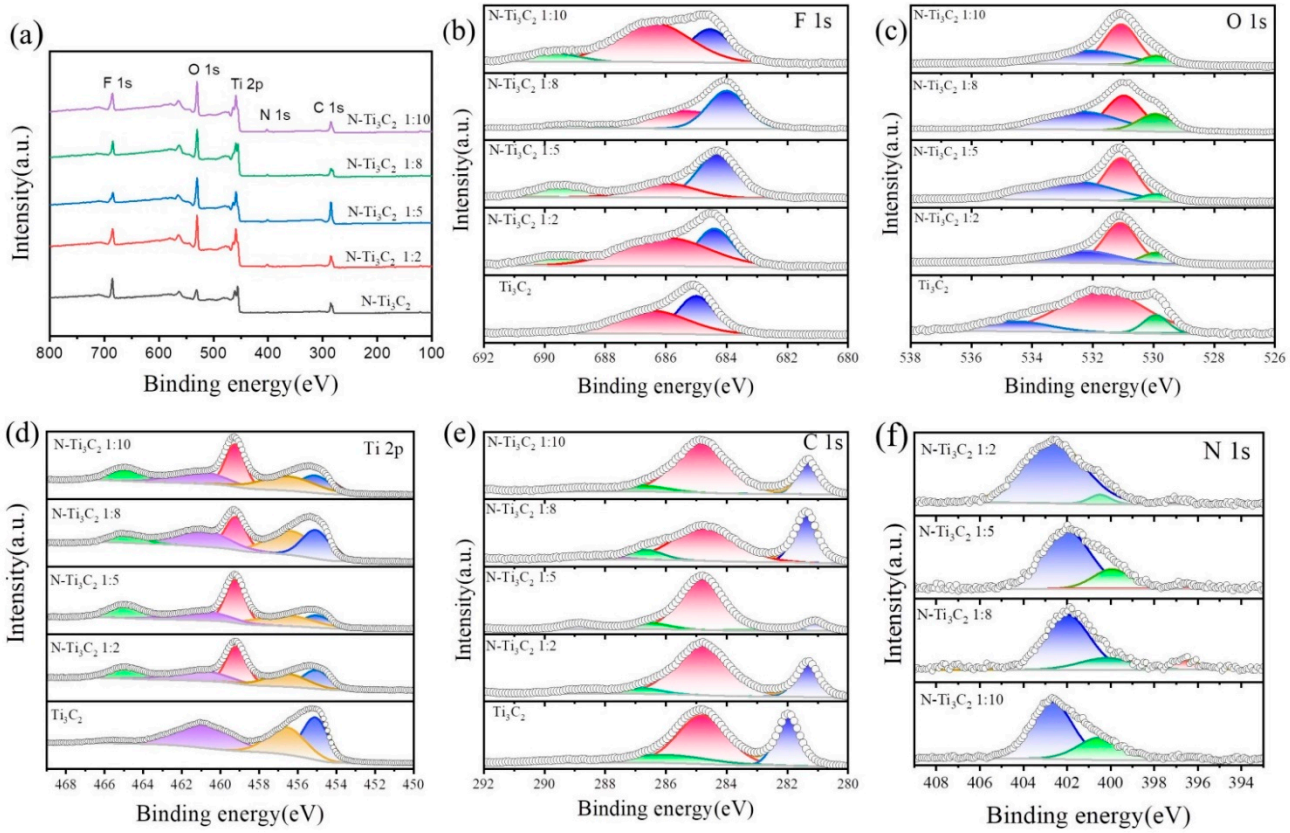

Figure 5. XPS spectra of the samples: (**a**) measurement scan, (**b**) F 1s, (**c**) O 1s, (**d**) Ti 2p, (**e**) C 1s, (**f**) N 1 s.

Figure 5f shows the XPS spectra of N 1s. Based on the high-resolution spectra of N 1 s, it can be shown that nitrogen is successfully doped into Ti_3C_2 and three peaks are identified near 396.58 eV, 400.18 eV, and 401.98 eV, which correspond to three nitrogen functional groups [15,35,46]: (i) nitride, abbreviated as N-Ti (396.58 eV), (ii) pyrrole nitrogen, abbreviated as N-5 (400.18 eV) and (iii) quaternary nitrogen, abbreviated as N-Q (401.98 eV). The peak at 396.58 eV originates from the substitution of nitrogen for carbon atoms to form mainly N-Ti (nitrides), which indicates that the N atom reacts not only with the C atom, but also bonds with the Ti atom. In contrast, the two peaks located near 400.18 eV and 401.98 eV originate from the -N functional group and surface adsorption, respectively [35]. It can be inferred that nitrogen is mainly present in the form of surface adsorption and pyrrole nitrogen (N-5), and the new peak found near 289.1 eV in the carbon elemental analysis spectrum also indicates the formation of the -N functional group.

3.4. Transient Photocurrent Response

Today, photocurrent is widely considered to be the most effective evidence for charge separation in heterogeneous structured photo-catalysts [42,47,48]. Typically, the value of photocurrent indirectly reflects the ability to generate and transfer photo-excited charge carriers under irradiation, which correlates with photo-catalytic activity.

Using the use of transient photocurrent response, the migration and separation traits of the photo-generated electron-hole pairs of the samples were examined. The transient photocurrent curves of N-Ti_3C_2 are shown in Figure 6. Among all the samples, the photocurrent of Ti_3C_2 was the highest, while the photocurrent of N-Ti_3C_2 1:8 was the lowest, and the photocurrent of Ti_3C_2 was much larger. The photocurrent magnitudes of Ti_3C_2 and N-Ti_3C_2 1:8 are not consistent with their photo-catalytic activities. It may occur as a result of the possibility that oxygen molecules adsorbed on the surface of N-Ti_3C_2 can interact with unbound electrons to form negatively charged O_2^-.

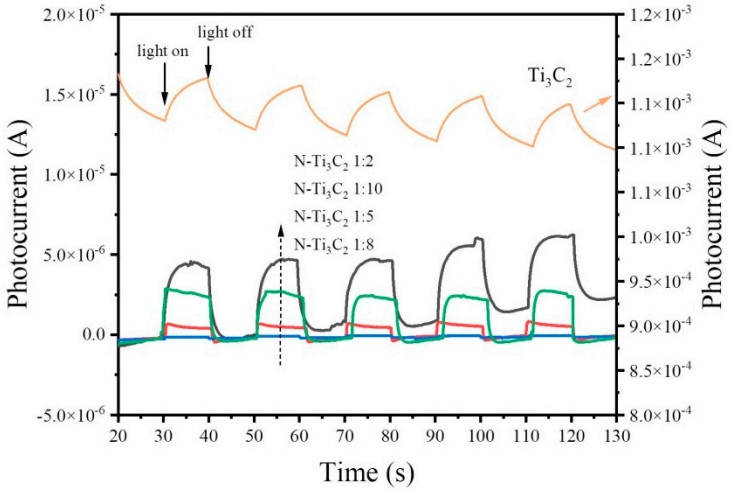

Figure 6. Transient photocurrents of Ti_3C_2 and N−Ti_3C_2 1:8.

It is known that the current is proportional to the mobility (μ) and density (n) of the charge carriers [49].

$$I = qn\mu FA$$

where q is the electron charge, F is the electric field, and A is the cross-sectional area. F and A were the same across all samples included in the investigation. This shows the great difference in material carrier mobility and that high photocurrent does not imply an abundant carrier density [50].

The transient photocurrent density of different samples was measured with three electrodes, and the order of the magnitude of photocurrent was Ti_3C_2 > N-Ti_3C_2 1:2 > N-Ti_3C_2 1:10 > N-Ti_3C_2 1:5 > N-Ti_3C_2 1:8, which is the opposite order of photo-catalytic activity, so it can be seen that there is no absolute relationship between the magnitude of photocurrent and photocatalytic activity.

3.5. Photocatalytic Degradation Activity and Cycling Experiments of MO

The photocatalytic ability of nitrogen-doped Ti_3C_2 MXene two-dimensional material was investigated by photocatalytic degradation of MO. The degradation efficiency was defined as $\eta = (C_0 - C_t)/C_0$, where C_0 is the initial concentration of methyl orange and C_t is the concentration of methyl orange at time t. Blank experiments with degradant solutions under the same conditions without a catalyst were also performed for comparison. In Figure 7a, Ti_3C_2 MXene materials with nitrogen doping ratios of 1:2, 1:5, 1:8, and 1:10 were tested. Compared to pure Ti_3C_2 MXene, N-Ti_3C_2 2D nanomaterials with high surface area and large pore volume due to N-Ti_3C_2 1:2, N-Ti_3C_2 1:5, N-Ti_3C_2 1:8 and N Ti_3C_2 1:10 two-dimensional nanomaterials all exhibited better photo-catalytic ability. Especially, N-Ti_3C_2 1:8 had the best photo-catalytic ability to degrade MO under UV light, and it degraded 98.73% of the methyl orange dye after 20 min of irradiation, and the removal rate of MO was 99.93% at 40 min. Figure 7b shows the pseudo-first-order kinetic plot of MO degradation with the equation: $-\ln(C_t/C_0) = kt$. Figure 7c depicts the kinetic rate constant (k) estimated using the pseudo-first-order kinetic model, as well as the variation of k for all samples visually, N-Ti_3C_2 1:2, N-Ti_3C_2 1:5, N-Ti_3C_2 1:8 and N-Ti_3C_2 1:10 for The kinetic rate constants for MO removal by 2D nanomaterials were 0.00574, 0.02387, 0.14669, 0.18717, and 0.02959 min^{-1}. The above results show that the N-Ti_3C_2 1:8 material shows the best photocatalytic performance with abundant active sites. The main reason may be that the nitrogen-doped materials have more abundant surface functional groups, which improve the charge transfer efficiency and enhance the electrical conductivity of the materials.

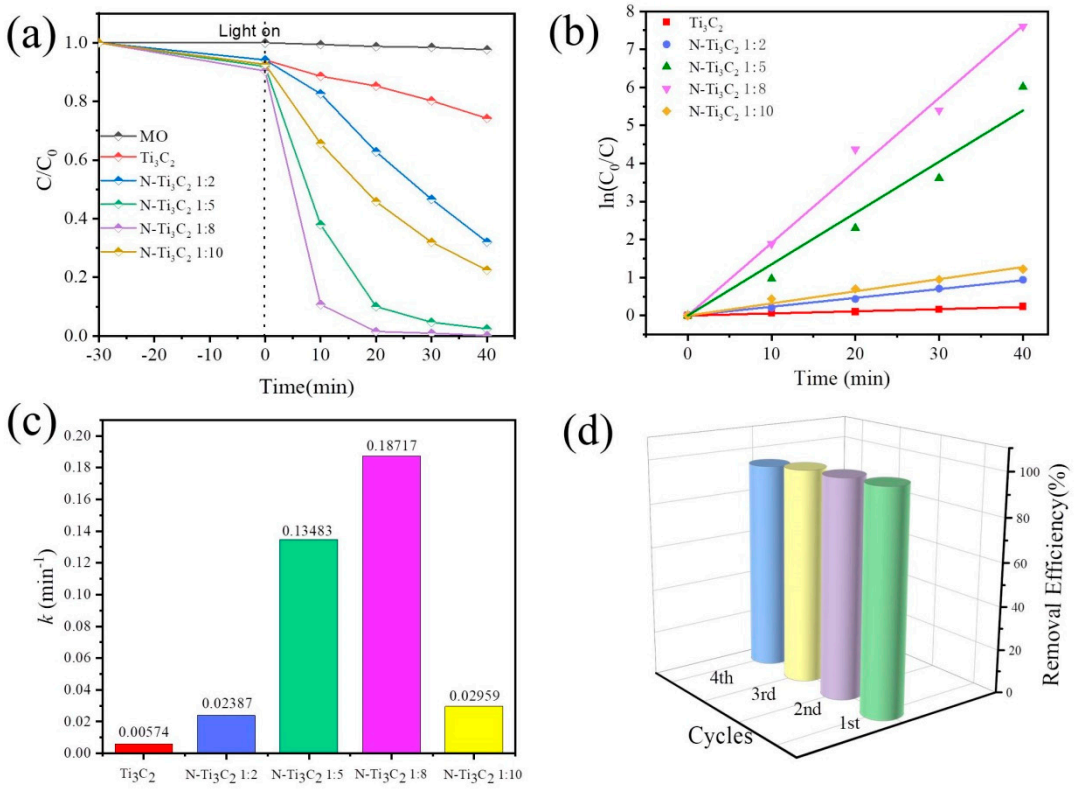

Figure 7. Photo-catalytic activity on (**a**) MO degradation activity, (**b**) pseudo-level diagram of MO degradation, (**c**) kinetic constants of MO degradation, (**d**) reusability of N−Ti_3C_2 1:8 for MO degradation.

In addition, the reusability of N-Ti_3C_2 1:8 2D nanomaterial was carried out to assess the stability. As seen in Figure 7d, the catalytic activity of the N-Ti_3C_2 1:8 2D nanomaterial for the degradation of methyl orange dye still reached 94.87% after four cycles. The catalytic degradation efficiency decreased only slightly after 4 cycles, and the slight decrease might be due to the loss of photocatalyst during the recovery process. The results demonstrate that the N-Ti_3C_2 1:8 two-dimensional nanomaterials have good chemical stability.

3.6. Effect of Dye Concentration on Degradation Rate

The experimental dye concentration gradient ranged from 20–60 mg/L, and it can be seen from Figure 8 that the photocatalytic degradation rate decreases sharply with the increase in dye concentration. There are two reasons for this: Firstly, at a certain amount of catalyst, the greater the concentration of dye, the slower the decrease in chromaticity, and the longer the time required for complete degradation [51]. Secondly, the solution light transmittance decreases with increasing dye concentration, the radiant energy absorbed by the catalyst decreases, and the photocatalytic efficiency becomes poor [52,53]. In addition, we also compared different two-dimensional material-based composite photocatalysts listed in Table 1.

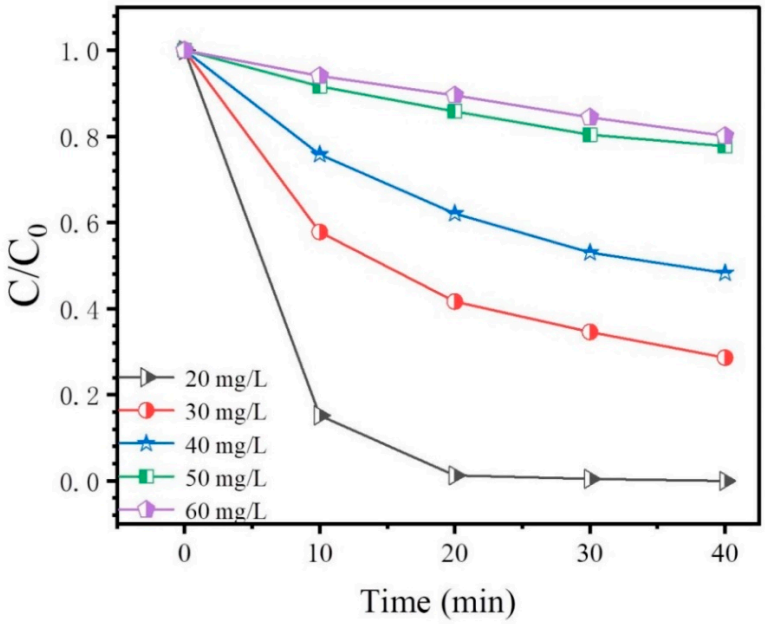

Figure 8. Effect of dye concentration on degradation rate.

Table 1. Represents the photo-catalytic activity of 2D material-based composite catalysts.

Composite	Light	Composite Mass	Dye	Time (min)	Degradation Rate	Ref.
(001)TiO_2/Ti_3C_2 (In-situ synthesis)	UV	10 mg	200 mL 20 mg/L Methyl orange (MO)	50	97.4%	[54]
$TiO_2/Ti_3C_2T_x$ (In-situ synthesis)	UV	-	MO	50	92%	[55]
$BiOI/Ti_3C_2$	Vis	20 mg	100 mL 10 mg/L RhB	30	99.8%	[31]
TiO_2/Ti_3C_2	UV	60 mg	60 mL 20 mg/L MO	40	99.6	[56]
TiO_2/Mxene	UV Vis	10 mg	20 mL 60 mg/L MB	60	96.44% 40.29%	[57]
g-$C_3N_4/TiO_2/Ti_3C_2$	Vis	50 mg	50 mL 20 mg/L MO	120	90.13%	[58]
Defect-Rich $Ti_3C_2/BiOIO_3$	Vis	10 mg	100 mL (10 mg/L) MO	40	97.6%	[59]
N-Ti_3C_2	UV	50 mg	50 mL 20 mg/L MO	40	99.93%	This work

3.7. Optical Properties

The UV-vis absorption properties and band gap of the materials were investigated by UV-vis diffuse reflectance spectroscopy. From Figure 9a, it can be seen that the absorption range of N-Ti_3C_2 is wider, and the absorption edge extends to 800 nm. The absorption of N-Ti_3C_2 is higher than that of Ti_3C_2, which is related to the doping of nitrogen elements. Moreover, a new absorption band appears at the position of the peak around 400 nm after nitrogen doping. Considering that the previous XRD and XPS tests showed the appearance of TiO_2 in the sample after nitrogen doping, this absorption should be caused by TiO_2. It can be seen from Figure 9b that nitrogen doping reduces the band gap, and the band gap of the material after N doping is reduced from 1.376 eV to 1.145 eV.

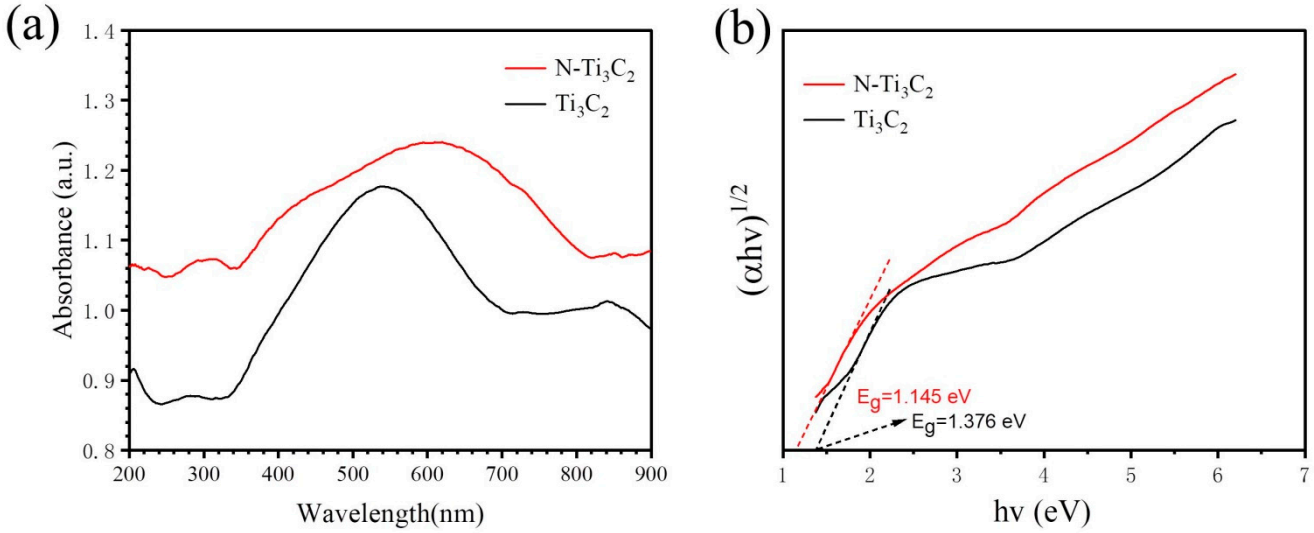

Figure 9. (**a**) Absorption spectra of Ti_3C_2 and N−Ti_3C_2 samples; (**b**) plots of $(\alpha h\nu)^{1/2}$ versus photon energy ($h\nu$) for band-gap energy.

3.8. Proposed Degradation Pathway and Photocatalytic Mechanism

In Figure 10, to further explore the photo-catalytic active substance, is to conduct a capture experiment of the active substance. In the degradation of MO by N-Ti_3C_2 1:8 2D nanomaterial, ethylenediaminetetraacetic acid disodium salt (EDTA-2Na) as a hole scavenger (h^+), isopropyl alcohol (IPA) as a hydroxyl radical (•OH) scavenger, sodium iodate ($NaIO_3$) as an electron (e^-) scavenger and p-benzoquinone (BQ) as superoxide radical ($\bullet O_2^-$) scavengers were analyzed for the active substances that play a major role in the photocatalytic degradation of methyl orange dye. The catalytic activity of N-Ti_3C_2 1:8 2D nanomaterial for MO degradation was found to be unaffected by the presence of EDTA-2Na, showing that the photo-catalytic active component was not h^+. And the catalytic activity decreased significantly after the addition of IPA, $NaIO_3$, and BQ, which proved that •OH, e^-, and $\bullet O_2^-$ were the photo-catalytic active substances that played the main role in the UV degradation of MO experiments.

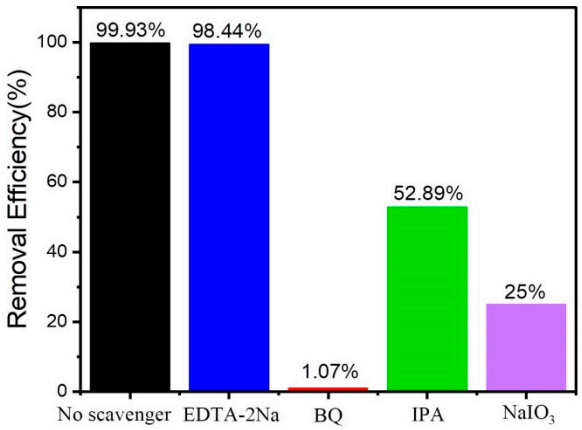

Figure 10. Shows the active substance capture experiment for the photo-degradation of MO by N-Ti_3C_2 1:8 nanomaterial.

Organic pollutants first diffuse from the contaminated solution to the surface of the photocatalyst and then desorb to the outer surface of the photocatalyst through effective adsorption and products of redox reactions. Based on the analysis of active substances, a speculative method to explain the photocatalytic activity of N-Ti_3C_2 material for the degradation of pollutants is proposed. As shown in Figure 11, Ti_3C_2 is recognized as a

material with excellent electrical conductivity, which can effectively separate electrons and holes and inhibit their complexation, and N doping further enhances this property. Photogenerated electrons and holes are generated on the surface of N-Ti_3C_2 MXene under the photoexcitation of UV light. And some of the photogenerated electrons on the conduction band of N-Ti_3C_2 MXene after photoexcitation are directly involved in the degradation of MO as a major active substance. Another part of photogenerated electrons reacts with O_2 to produce the active substance superoxide radical ($\bullet O_2^-$) to participate in the degradation process of MO. The other part of photogenerated electrons reacts with O_2 to produce the reactive substance superoxide radical ($\bullet O_2^-$) to participate in the degradation process of MO [60]. The photogenerated holes left in the valence band react with adsorbed hydroxide ions (OH^-) and H_2O to produce hydroxyl radicals ($\bullet$OH), allowing the oxidation of organic pollutants by $\bullet$OH [61,62]. These highly reactive species ($\bullet O_2^-$, $\bullet$OH, and e^-) enable rapid photodegradation of MO under UV light irradiation. This is in agreement with our active species capture experiment Figure 10.

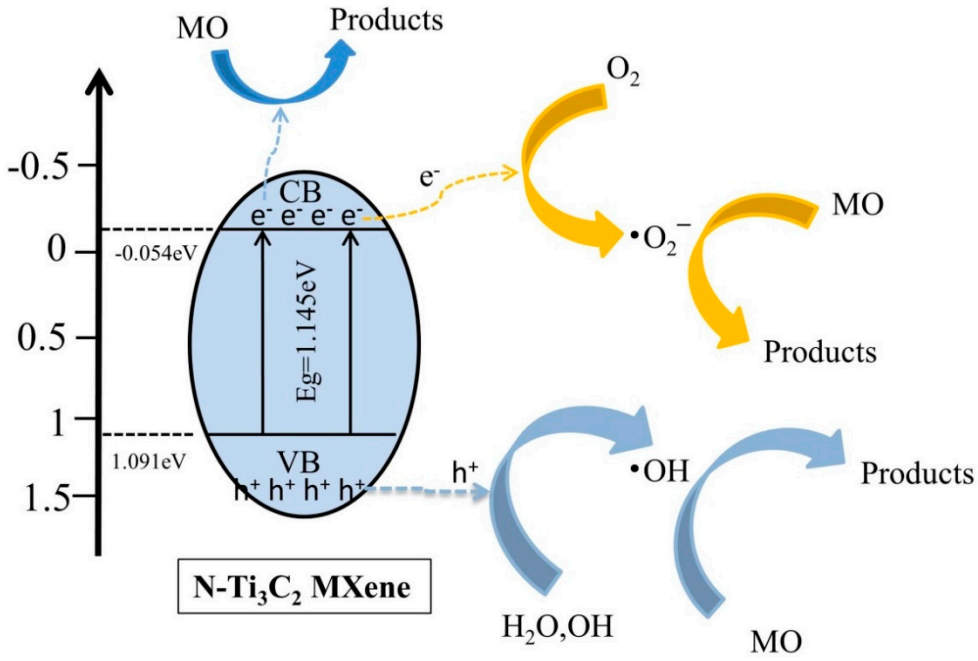

Figure 11. Photocatalytic degradation mechanism of N-Ti_3C_2 MXene.

4. Conclusions, Ongoing Challenges, and Perspective

In this work, N-Ti_3C_2 MXene two-dimensional nanomaterials were prepared by a facile and controllable strategy combining solvent heat treatment and non-in situ nitrogen doping using urea-saturated alcohol solution as a liquid nitrogen source. Its methyl orange dye removal rate was 98.73% after 20 min of UV lamp irradiation, and it still had good photo-catalytic activity after four cycles. N-doped Ti_3C_2 MXene would not only provide an effective electron transfer pathway but also increase the interlayer distance of MXene and expose more active sites, thus showing extraordinary photo-catalytic performance in pollutant degradation. Moreover, it further demonstrates that the electrical conductivity of N-Ti_3C_2 MXene can effectively transfer photo-generated electrons, resulting in a large amount of photo-catalytically active substances ($\bullet$OH, e^-, and $\bullet O_2^-$). Therefore, N-Ti_3C_2 MXene two-dimensional nanomaterial can be used as an effective and promising photo-catalyst for wastewater purification.

For the present, there are some limitations to this work. The excitation light source used during the experiments is UV light, which is more energetic, and the organic pollutants degraded in the photo-catalytic study are relatively single. The cycling experiments have not yet reached efficiency saturation. There is a need to further explore the photocatalytic activity of N-Ti_3C_2 MXene under sunlight or visual light to degrade a variety of organic

pollutants, such as antibiotics. And the photo-catalytic cycle of the material needs to be further investigated until the cycling efficiency is saturated. In addition, a toxicity assessment of the treated solution is needed to ensure that the discharged wastewater will reduce the adverse environmental impact.

Author Contributions: Writing—original draft, L.C.; Investigation, Date curation, Validation, Q.D. and X.D.; Conceptualization, Methodology, J.X. and T.T.; Formal analysis, Visualization, Validation, G.H., X.C. and L.J.; Project administration, Funding acquisition, Conceptualization, M.L.; Writing—review & editing, Supervision, Methodology, J.W. and Y.Y. All authors have read and agreed to the published version of the manuscript.

Funding: This work was supported by the Guangxi Graduate Education Innovation Project (No. YCSW2022331).

Institutional Review Board Statement: Not applicable.

Informed Consent Statement: Not applicable.

Data Availability Statement: Not applicable.

Conflicts of Interest: The authors declare no conflict of interest.

References

1. Patnaik, S.; Das, K.K.; Mohanty, A.; Parida, K. Enhanced photo catalytic reduction of Cr (VI) over polymer-sensitized g-C_3N_4/$ZnFe_2O_4$ and its synergism with phenol oxidation under visible light irradiation. *Catal. Today* **2018**, *315*, 52–66. [CrossRef]
2. Pronk, W.; Ding, A.; Morgenroth, E.; Derlon, N.; Desmond, P.; Burkhardt, M.; Wu, B.; Fane, A.G. Gravity-driven membrane filtration for water and wastewater treatment: A review. *Water Res.* **2019**, *149*, 553–565. [CrossRef] [PubMed]
3. Wang, R.; Yang, R.; Zhang, Y. A study of applying green glucose-reduced graphene oxide in advanced treatment of different dyes. *Desalin. Water Treat* **2017**, *70*, 387–393. [CrossRef]
4. Sun, S.; Liu, P.; Ullah, M. Efficient Azo Dye Biodecolorization System Using Lignin-Co-Cultured White-Rot Fungus. *J. Fungi* **2023**, *9*, 91. [CrossRef]
5. Ndlovu, L.N.; Malatjie, K.I.; Donga, C.; Mishra, A.K.; Nxumalo, E.N.; Mishra, S.B. Catalytic degradation of methyl orange using beta cyclodextrin modified polyvinylidene fluoride mixed matrix membranes imbedded with in-situ generated palladium nanoparticles. *J. Appl. Polym. Sci.* **2023**, *140*, e53270. [CrossRef]
6. Jia, Z.; Wang, Q.; Sun, L.; Wang, Q.; Zhang, L.C.; Wu, G.; Luan, J.H.; Jiao, Z.B.; Wang, A.; Liang, S.X. Attractive in situ self-reconstructed hierarchical gradient structure of metallic glass for high efficiency and remarkable stability in catalytic performance. *Adv. Funct. Mater.* **2019**, *29*, 1807857. [CrossRef]
7. Zhang, L.; Li, Y.; Guo, H.; Zhang, H.; Zhang, N.; Hayat, T.; Sun, Y. Decontamination of U (VI) on graphene oxide/Al_2O_3 composites investigated by XRD, FT-IR and XPS techniques. *Environ. Pollut.* **2019**, *248*, 332–338. [CrossRef]
8. Huang, H.; Song, Y.; Li, N.; Chen, D.; Xu, Q.; Li, H.; He, J.; Lu, J. One-step in-situ preparation of N-doped TiO_2@ C derived from Ti_3C_2 MXene for enhanced visible-light driven photodegradation. *Appl. Catal. B* **2019**, *251*, 154–161. [CrossRef]
9. Rameshbabu, R.; Neppolian, B. Surfactant assisted hydrothermal synthesis of superparamagnetic $ZnFe_2O_4$ nanoparticles as an efficient visible-light photocatalyst for the degradation of organic pollutant. *J. Clust. Sci.* **2016**, *27*, 1977–1987. [CrossRef]
10. Im, J.K.; Sohn, E.J.; Kim, S.; Jang, M.; Son, A.; Zoh, K.-D.; Yoon, Y. Review of MXene-based nanocomposites for photocatalysis. *Chemosphere* **2021**, *270*, 129478. [CrossRef]
11. Huang, K.; Li, C.; Li, H.; Ren, G.; Wang, L.; Wang, W.; Meng, X. Photocatalytic Applications of Two-Dimensional Ti_3C_2 MXenes: A Review. *ACS Appl. Nano Mater.* **2020**, *3*, 9581–9603. [CrossRef]
12. Shukla, S.; Kang, S.-Y.; Saxena, S. Synthesis and patterning of graphene: Strategies and prospects. *Appl. Phys. Rev.* **2019**, *6*, 021311. [CrossRef]
13. Naguib, M.; Mochalin, V.N.; Barsoum, M.W.; Gogotsi, Y. 25th anniversary article: MXenes: A new family of two-dimensional materials. *Adv. Mater.* **2014**, *26*, 992–1005. [CrossRef]
14. Neupane, G.P.; Yildirim, T.; Zhang, L.; Lu, Y. Retracted: Emerging 2D MXene/Organic Heterostructures for Future Nanodevices. *Adv. Funct. Mater.* **2020**, *30*, 2005238. [CrossRef]
15. Chaudhari, N.K.; Jin, H.; Kim, B.; San Baek, D.; Joo, S.H.; Lee, K. MXene: An emerging two-dimensional material for future energy conversion and storage applications. *J. Mater. Chem. A* **2017**, *5*, 24564–24579. [CrossRef]
16. Tang, Y.; Yang, C.; Tian, Y.; Luo, Y.; Yin, X.; Que, W. The effect of in situ nitrogen doping on the oxygen evolution reaction of MXenes. *Nanoscale Adv.* **2020**, *2*, 1187–1194. [CrossRef]
17. Huang, W.-X.; Li, Z.-P.; Li, D.-D.; Hu, Z.-H.; Wu, C.; Lv, K.-L.; Li, Q. Ti_3C_2 MXene: Recent progress in its fundamentals, synthesis, and applications. *Rare Met.* **2022**, *41*, 3268–3300. [CrossRef]
18. Naguib, M.; Kurtoglu, M.; Presser, V.; Lu, J.; Niu, J.; Heon, M.; Hultman, L.; Gogotsi, Y.; Barsoum, M.W. Two-dimensional nanocrystals produced by exfoliation of Ti_3AlC_2. *Adv. Mater.* **2011**, *23*, 4248–4253. [CrossRef] [PubMed]

19. Khazaei, M.; Mishra, A.; Venkataramanan, N.S.; Singh, A.K.; Yunoki, S. Recent advances in MXenes: From fundamentals to applications. *Curr. Opin. Solid State Mater. Sci.* **2019**, *23*, 164–178. [CrossRef]
20. Peng, C.; Wei, P.; Chen, X.; Zhang, Y.; Zhu, F.; Cao, Y.; Wang, H.; Yu, H.; Peng, F. A hydrothermal etching route to synthesis of 2D MXene (Ti_3C_2, Nb_2C): Enhanced exfoliation and improved adsorption performance. *Ceram. Int.* **2018**, *44*, 18886–18893. [CrossRef]
21. Maeda, K.; Wakayama, H.; Washio, Y.; Ishikawa, A.; Okazaki, M.; Nakata, H.; Matsuishi, S. Visible-light-induced photocatalytic activity of stacked MXene sheets of Y_2CF_2. *J. Phys. Chem. C* **2020**, *124*, 14640–14645. [CrossRef]
22. Ghidiu, M.; Lukatskaya, M.R.; Zhao, M.-Q.; Gogotsi, Y.; Barsoum, M.W. Conductive two-dimensional titanium carbide 'clay'with high volumetric capacitance. *Nature* **2014**, *516*, 78–81. [CrossRef] [PubMed]
23. Peng, J.; Chen, X.; Ong, W.-J.; Zhao, X.; Li, N. Surface and heterointerface engineering of 2D MXenes and their nanocomposites: Insights into electro-and photocatalysis. *Chemistry* **2019**, *5*, 18–50. [CrossRef]
24. Zhao, D.; Chen, Z.; Yang, W.; Liu, S.; Zhang, X.; Yu, Y.; Cheong, W.-C.; Zheng, L.; Ren, F.; Ying, G. MXene (Ti_3C_2) vacancy-confined single-atom catalyst for efficient functionalization of CO_2. *J. Am. Chem. Soc.* **2019**, *141*, 4086–4093. [CrossRef] [PubMed]
25. Ronchi, R.M.; Arantes, J.T.; Santos, S.F. Synthesis, structure, properties and applications of MXenes: Current status and perspectives. *Ceram. Int.* **2019**, *45*, 18167–18188. [CrossRef]
26. Sinopoli, A.; Othman, Z.; Rasool, K.; Mahmoud, K.A. Electrocatalytic/photocatalytic properties and aqueous media applications of 2D transition metal carbides (MXenes). *Curr. Opin. Solid State Mater. Sci.* **2019**, *23*, 100760. [CrossRef]
27. Abid, A.; Idrees, M.; Din, H.U.; Alam, Q.; Amin, B.; Haneef, M. Structural, electronic, optical, thermoelectric and photocatalytic properties of SiS/MXenes van der Waals heterostructures. *Mater. Today Commun.* **2021**, *26*, 101702. [CrossRef]
28. Li, S.; Wang, Y.; Wang, J.; Liang, J.; Li, Y.; Li, P. Modifying g-C_3N_4 with oxidized Ti_3C_2 MXene for boosting photocatalytic U (VI) reduction performance. *J. Mol. Liq.* **2022**, *346*, 117937. [CrossRef]
29. Li, K.; Zhang, S.; Li, Y.; Fan, J.; Lv, K. MXenes as noble-metal-alternative co-catalysts in photocatalysis. *Chin. J. Catal.* **2021**, *42*, 3–14. [CrossRef]
30. Huang, K.; Li, C.; Wang, L.; Wang, W.; Meng, X. Layered Ti_3C_2 MXene and silver co-modified g-C_3N_4 with enhanced visible light-driven photocatalytic activity. *Chem. Eng. J.* **2021**, *425*, 131493. [CrossRef]
31. Zhang, H.; Li, M.; Wang, W.; Zhang, G.; Tang, Q.; Cao, J. Designing 3D porous BiOI/Ti_3C_2 nanocomposite as a superior coating photocatalyst for photodegradation RhB and photoreduction Cr (VI). *Sep. Purif. Technol.* **2021**, *272*, 118911. [CrossRef]
32. Hu, X.; Wang, Y.; Ling, Z.; Song, H.; Cai, Y.; Li, Z.; Zu, D.; Li, C. Ternary g-C_3N_4/TiO_2/Ti_3C_2 MXene S-scheme heterojunction photocatalysts for NOx removal under visible light. *Appl. Surf. Sci.* **2021**, *556*, 149817. [CrossRef]
33. Tang, R.; Xiong, S.; Gong, D.; Deng, Y.; Wang, Y.; Su, L.; Ding, C.; Yang, L.; Liao, C. Ti_3C_2 2D MXene: Recent Progress and Perspectives in Photocatalysis. *ACS Appl. Mater. Interfaces* **2020**, *12*, 56663–56680. [CrossRef]
34. Zhang, X.; Zhang, Z.; Zhou, Z. MXene-based materials for electrochemical energy storage. *J. Energy Chem.* **2018**, *27*, 73–85. [CrossRef]
35. Yang, C.; Tang, Y.; Tian, Y.; Luo, Y.; Faraz Ud Din, M.; Yin, X.; Que, W. Flexible nitrogen-doped 2D titanium carbides (MXene) films constructed by an ex situ solvothermal method with extraordinary volumetric capacitance. *Adv. Energy Mater.* **2018**, *8*, 1802087. [CrossRef]
36. Jin, Y.; Ao, H.; Qi, K.; Zhang, X.; Liu, M.; Zhou, T.; Wang, S.; Xia, G.; Zhu, Y. A high-rate, long life, and anti-self-discharge aqueous N-doped Ti_3C_2/Zn hybrid capacitor. *Mater. Today Energy* **2021**, *19*, 100598. [CrossRef]
37. Wang, J.; Zhang, Z.; Yan, X.; Zhang, S.; Wu, Z.; Zhuang, Z.; Han, W.-Q. Rational design of porous N-Ti_3C_2 MXene@ CNT microspheres for high cycling stability in Li–S battery. *Nanomicro Lett.* **2020**, *12*, 1–14. [CrossRef] [PubMed]
38. Ashraf, I.; Ahmad, S.; Dastan, D.; Wang, C.; Garmestani, H.; Iqbal, M. Delaminated N-Ti_3C_2@ Ni_3S_4 Nanocomposites based High-Performing Supercapacitor Device Fabrication. *Electrochim. Acta* **2023**, *441*, 141899. [CrossRef]
39. Kang, Z.; Cai, J.; Ye, D.; Zhao, H.; Luo, J.; Zhang, J. Three-dimensional nitrogen-doped MXene as support to form high-performance platinum catalysts for water-electrolysis to produce hydrogen. *Chem. Eng. J.* **2022**, *446*, 137443. [CrossRef]
40. Kibasomba, P.M.; Dhlamini, S.; Maaza, M.; Liu, C.-P.; Rashad, M.M.; Rayan, D.A.; Mwakikunga, B.W. Strain and grain size of TiO_2 nanoparticles from TEM, Raman spectroscopy and XRD: The revisiting of the Williamson-Hall plot method. *Results Phys.* **2018**, *9*, 628–635. [CrossRef]
41. Ding, Z.; Sun, M.; Liu, W.; Meng, X.; Zheng, Y.; Sun, W.; Zhou, Q. In-situ growth of N–TiO_2 on delaminated N–Ti_3C_2 with highly strengthened photocatalytic activity. *Int. J. Hydrogen Energy* **2022**, *47*, 21204–21219. [CrossRef]
42. Natu, V.; Benchakar, M.; Canaff, C.; Habrioux, A.; Celerier, S.; Barsoum, M.W. A critical analysis of the X-ray photoelectron spectra of $Ti_3C_2T_z$ MXenes. *Matter* **2021**, *4*, 1224–1251. [CrossRef]
43. Meng, Y.; Li, Y.; Xia, J.; Hu, Q.; Ke, X.; Ren, G.; Zhu, F. F-doped $LiFePO_4$@ N/B/F-doped carbon as high performance cathode materials for Li-ion batteries. *Appl. Surf. Sci.* **2019**, *476*, 761–768. [CrossRef]
44. Hui, X.; Ge, X.; Zhao, R.; Li, Z.; Yin, L. Interface chemistry on MXene-based materials for enhanced energy storage and conversion performance. *Adv. Funct. Mater.* **2020**, *30*, 2005190. [CrossRef]
45. Lu, C.; Yang, L.; Yan, B.; Sun, L.; Zhang, P.; Zhang, W.; Sun, Z. Nitrogen-doped Ti_3C_2 MXene: Mechanism investigation and electrochemical analysis. *Adv. Funct. Mater.* **2020**, *30*, 2000852. [CrossRef]
46. Han, M.; Yang, J.; Jiang, J.; Jing, R.; Ren, S.; Yan, C. Efficient tuning the electronic structure of N-doped Ti-based MXene to enhance hydrogen evolution reaction. *J. Colloid Interface Sci.* **2021**, *582*, 1099–1106. [CrossRef]

47. Kim, H.-i.; Kim, J.; Kim, W.; Choi, W. Enhanced photocatalytic and photoelectrochemical activity in the ternary hybrid of $CdS/TiO_2/WO_3$ through the cascadal electron transfer. *J. Phys. Chem. C* **2011**, *115*, 9797–9805. [CrossRef]
48. Xu, Q.C.; Wellia, D.V.; Ng, Y.H.; Amal, R.; Tan, T.T.Y. Synthesis of porous and visible-light absorbing Bi_2WO_6/TiO_2 heterojunction films with improved photoelectrochemical and photocatalytic performances. *J. Phys. Chem. C* **2011**, *115*, 7419–7428. [CrossRef]
49. Nelson, J.; Eppler, A.M.; Ballard, I.M. Photoconductivity and charge trapping in porous nanocrystalline titanium dioxide. *J. Photochem. Photobiol. A* **2002**, *148*, 25–31. [CrossRef]
50. Liu, Y.; Xie, C.; Li, J.; Zou, T.; Zeng, D. New insights into the relationship between photocatalytic activity and photocurrent of TiO_2/WO_3 nanocomposite. *Appl. Catal. A* **2012**, *433*, 81–87. [CrossRef]
51. Chen, X.; Wu, Z.; Liu, D.; Gao, Z. Preparation of ZnO photocatalyst for the efficient and rapid photocatalytic degradation of azo dyes. *Nanoscale Res. Lett.* **2017**, *12*, 1–10. [CrossRef] [PubMed]
52. Mehrabi, M.; Javanbakht, V. Photocatalytic degradation of cationic and anionic dyes by a novel nanophotocatalyst of $TiO_2/ZnTiO_3/\alpha Fe_2O_3$ by ultraviolet light irradiation. *J. Mater. Sci. Mater. Electron.* **2018**, *29*, 9908–9919. [CrossRef]
53. Hieu, V.Q.; Phung, T.K.; Nguyen, T.-Q.; Khan, A.; Doan, V.D.; Tran, V.A. Photocatalytic degradation of methyl orange dye by Ti_3C_2–TiO_2 heterojunction under solar light. *Chemosphere* **2021**, *276*, 130154. [CrossRef]
54. Peng, C.; Yang, X.; Li, Y.; Yu, H.; Wang, H.; Peng, F. Hybrids of two-dimensional Ti_3C_2 and TiO_2 exposing {001} facets toward enhanced photocatalytic activity. *ACS Appl. Mater. Interfaces* **2016**, *8*, 6051–6060. [CrossRef]
55. Chen, J.; Zheng, H.; Zhao, Y.; Que, M.; Lei, X.; Zhang, K.; Luo, Y. Preparation of facet exposed $TiO_2/Ti_3C_2T_x$ composites with enhanced photocatalytic activity. *J. Phys. Chem. Solids* **2020**, *145*, 109565. [CrossRef]
56. Li, H.; Sun, B.; Gao, T.; Li, H.; Ren, Y.; Zhou, G. Ti_3C_2 MXene co-catalyst assembled with mesoporous TiO_2 for boosting photocatalytic activity of methyl orange degradation and hydrogen production. *Chin. J. Catal.* **2022**, *43*, 461–471. [CrossRef]
57. Zhang, S.; Cai, M.; Wu, J.; Wang, Z.; Lu, X.; Li, K.; Lee, J.-M.; Min, Y. photocatalytic degradation of TiO_2 via incorporating Ti_3C_2 MXene for methylene blue removal from water. *Catal. Commun.* **2023**, *174*, 106594. [CrossRef]
58. Luo, M.; Feng, H.; Hu, Y.; Chen, K.; Dong, Z.; Xue, S. Visible Light Induced $g\text{-}C_3N_4/TiO_2/Ti_3C_2$ Ternary Z-scheme Heterojunction Photocatalyst for Efficient Degradation. *Electron. Mater. Lett.* **2023**, *19*, 94–107. [CrossRef]
59. Chen, D.; Li, Y.; Xu, H.; Wang, A.; Liu, K. Interfacial Charge Transfer in Defect-Rich $Ti_3C_2/BiOIO_3$ Heterostructured Photocatalysts for the Degradation of Methyl Orange. *ACS Appl. Nano Mater.* **2022**, *5*, 18178–18187. [CrossRef]
60. Xu, R.; Wei, N.; Li, Z.; Song, X.; Li, Q.; Sun, K.; Yang, E.; Gong, L.; Sui, Y.; Tian, J. Construction of hierarchical 2D/2D Ti_3C_2/MoS_2 nanocomposites for high-efficiency solar steam generation. *J. Colloid Interface Sci.* **2021**, *584*, 125–133. [CrossRef]
61. Sun, B.; Qiu, P.; Liang, Z.; Xue, Y.; Zhang, X.; Yang, L.; Cui, H.; Tian, J. The fabrication of 1D/2D CdS nanorod@ Ti_3C_2 MXene composites for good photocatalytic activity of hydrogen generation and ammonia synthesis. *Chem. Eng. J.* **2021**, *406*, 127177. [CrossRef]
62. Tran, V.A.; Kadam, A.N.; Lee, S.-W. Adsorption-assisted photocatalytic degradation of methyl orange dye by zeolite-imidazole-framework-derived nanoparticles. *J. Alloys Compd.* **2020**, *835*, 155414. [CrossRef]